Neuro-Oncology Advances

5(1), 1–14, 2023 | https://doi.org/10.1093/noajnl/vdad111 | Advance Access date 12 September 2023

MRI-guided focused ultrasound blood–brain barrier opening increases drug delivery and efficacy in a diffuse midline glioma mouse model

Payton Martinez, Genna Nault, Jenna Steiner, Michael F. Wempe, Angela Pierce, Breauna Brunt, Mathew Slade, Jane J. Song, Andrew Mongin, Kang-Ho Song, Nicholas Ellens, Natalie Serkova, Adam L. Green, and Mark Borden

Biomedical Engineering Program, University of Colorado Boulder, Boulder, Colorado, USA (P.M., J.J.S., A.M., M.B.); Department of Mechanical Engineering, University of Colorado Boulder, Boulder, Colorado, USA (P.M., J.J.S., K.S., M.B.); Department of Radiology, Animal Imaging Shared Resource, University of Colorado Anschutz Medical Campus, Aurora, Colorado, USA (G.N., J.S., N.S.); Department of Pharmacy and Pharmaceutical Sciences, University of Colorado Anschutz Medical Campus, Aurora, Colorado, USA (M.F.W.); Morgan Adams Foundation Pediatric Brain Tumor Research Program, Department of Pediatrics, University of Colorado School of Medicine, Aurora, Colorado, USA (A.P., B.B., M.S., A.G.); Alpheus Medical, Inc., Chanhassen, Minnesota, USA (N.E.); Acertara Acoustic Labs, Longmont, Colorado, USA (N.E.)

Corresponding Authors: Adam Green, MD, University of Colorado Anschutz Medical Campus, 12800 E. 19th Ave., Mail Stop 8302, Aurora, CO 80045, USA (adam.green@cuanschutz.edu); Mark Borden, PhD, University of Colorado Boulder, 1111 Engineering Drive, Boulder, CO80309, USA (mark.borden@colorado.edu).

Abstract

Background. Diffuse intrinsic pontine glioma (DIPG) is the most common and deadliest pediatric brainstem tumor and is difficult to treat with chemotherapy in part due to the blood–brain barrier (BBB). Focused ultrasound (FUS) and microbubbles (MBs) have been shown to cause BBB opening, allowing larger chemotherapeutics to enter the parenchyma. Panobinostat is an example of a promising in vitro agent in DIPG with poor clinical efficacy due to low BBB penetrance. In this study, we hypothesized that using FUS to disrupt the BBB allows higher concentrations of panobinostat to accumulate in the tumor, providing a therapeutic effect.

Methods. Mice were orthotopically injected with a patient-derived diffuse midline glioma (DMG) cell line, BT245. MRI was used to guide FUS/MB (1.5 MHz, 0.615 MPa peak negative pressure, 1 Hz pulse repetition frequency, 10-ms pulse length, 3 min treatment time)/(25 µL/kg, i.v.) targeting to the tumor location.

Results. In animals receiving panobinostat (10 mg/kg, i.p.) in combination with FUS/MB, a 3-fold increase in tumor panobinostat concentration was observed, without significant increase of the drug in the forebrain. In mice receiving 3 weekly treatments, the combination of panobinostat and FUS/MB led to a 71% reduction of tumor volumes ($P = .01$). Furthermore, we showed the first survival benefit from FUS/MB improved delivery increasing the mean survival from 21 to 31 days ($P < .0001$).

Conclusions. Our study demonstrates that FUS-mediated BBB disruption can increase the delivery of panobinostat to an orthotopic DMG tumor, providing a strong therapeutic effect and increased survival.

Key Points

- In a patient-derived xenograft diffuse midline glioma tumor model, we showed that MRI-guided focused ultrasound (MRIgFUS) is safe and effective over multiple treatments.
- MRgFUS more effectively delivers panobinostat precisely to the tumor region.
- Weekly treatments of MRgFUS and panobinostat showed reduced tumor growth and increased survival.

Graphical Abstract

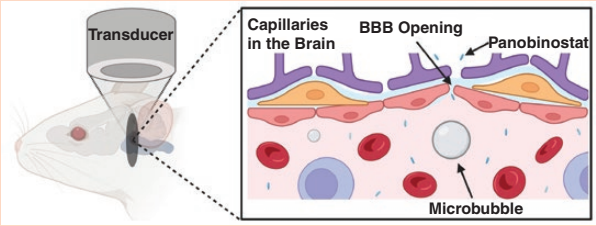

Importance of the Study

Diffuse midline gliomas, particularly diffuse intrinsic pontine glioma (DIPG), have remained a major clinical challenge to treat given their location and intact blood–brain barrier (BBB). Larger therapeutics with great in vitro potential including panobinostat are unable to cross at effective doses. MRI-guided focused ultrasound (MRIgFUS) is a technique to open the BBB noninvasively and temporarily at a targeted focal region. We have shown that FUS/microbubbles (MBs) can safely open the BBB and allow significantly more panobinostat to enter the tumor site. Our treatment parameters illustrated a similar extent of BBB opening over 3 weeks. Moreover, we illustrated a significant survival benefit for the FUS/MB-treated group compared to the panobinostat only group. This approach provides a pathway to deliver more effective chemotherapeutics to diffuse midline gliomas while maintaining safety and efficacy over multiple treatments. This work is a critical preclinical step to inform the use of this technology for DIPG patients in human clinical trials.

In 1926, Wilfred Harris first described diffuse intrinsic pontine glioma (DIPG) affecting the pontine area of the brainstem. To this day, DIPG remains one of the most difficult brain tumors to treat.[1] Imaging is crucial for establishing DIPG diagnosis, with MRI considered as the gold standard.[2] Further classification is made through genetic sequencing of biopsies taken from patients; it has been shown that over 80% of DIPG share a similar somatic gain-of-function mutation, where a missense substitution is found for lysine 27 to methionine in either histone variant HIST1H3B (H3.1) or H3F3A (H3.3).[3] The World Health Organization (WHO) recently classified DIPGs and other midline tumors with this mutation as "H3 K27M-altered diffuse midline gliomas (DMG)".[4] The proposed mechanism behind this variation is overexpression of EZH inhibitory protein (EZHIP), which acts similarly to the K27M mutation that inhibits the polycomb repressive complex 2 (PRC2).[5,6] With this information, considerable research has been done to find epigenetic modifiers. These technologies include inhibiting EZH2,[7,8] histone deacetylase inhibitors[1,9] and H327 demethylase or methyltransferase to target trimethylation.[10] Many cytotoxic[7,8] and targeted[9,11] drugs have been the subject of DMG clinical trials. Unfortunately, none of these drugs have worked in clinical studies owing in part to the impermeability of the tumor blood–brain barrier (BBB).[12,13]

One major obstacle to the efficacy of current treatments is the low accumulation of drugs in the tumor region. The pons, has an intact BBB that prevents most chemotherapies from entering the parenchyma. Moreover, the pons possesses a more unyielding BBB, further complicating the penetration of pharmaceuticals.[14] An impermeable blood–brain tumor barrier (BBTB) also limits the tumor margin visibility on T1-weighted contrast-enhanced (CE) MRI scans.[15] A study by McCully et al. showed that the BBTB is not homogeneous, as there was a difference in temozolomide penetration between the brainstem and pons regions relative to the cortex.[14] While there are a few chemotherapeutic agents, including gemcitabine, that have shown the ability to penetrate the BBTB in a human pontine DMG,[16] unfortunately these agents have not improved outcomes. Therefore, delivery methods are needed to enhance drug efficacy in these tumors.

One drug delivery technique that has been used to address this issue is convection-enhanced delivery (CED). This method has shown higher therapeutic penetrance at the target site with less systemic toxicity.[17,18] However, CED can present complications, especially in solid tumors. Some tumors are highly vascularized, high interstitial pressure, and less susceptible to the pressure-driven approach.[19] Alternatively, quickly growing tumors can develop areas of necrosis, rendering CED less effective as drugs can pool preventing delivery to the faster-growing cells on the periphery.[20] The invasiveness of this technique is also a concern, as it requires surgery to pierce through the scalp, skull, dura, and healthy brain tissue to place the catheter(s). Furthermore, clinical trials have shown the potential for an increase in neurological damage at higher CED flow rates.[21]

Focused ultrasound complemented with microbubbles (FUS/MB) has materialized as a noninvasive technique to disrupt the BBB in a targeted and reversible fashion.[22–25]

Microbubbles utilized for this technique were originally developed and clinically approved as ultrasound contrast agents. They are typically 1–10 μm diameter, with a shell (eg, lipid or protein) that encapsulates a high-molecular-weight gas (eg, perfluorocarbon).[26,27] The physical mechanism is that the circulating, gas-filled microbubbles expand and contract under the exposure of ultrasonic pressure waves (0.2–2 MHz) far more than the surrounding fluid and viscoelastic tissue. As a result, the local mechanical forces cause the separation of tight junctions, disrupting the BBB.[28,29] Researchers have classified 2 types of cavitation based on their acoustic echo: harmonic and inertial. Harmonic cavitation is characterized by relatively small oscillations and produces a frequency response at harmonics of the driving frequency.[30,31] The sub- and ultraharmonic responses are caused by the nonlinearity of the microbubbles as they cavitate.[30] Inertial cavitation can be described as violent expansion and contraction producing a broadband frequency response due to shock waves generated by microbubble implosions.[31] Both regimes of cavitation produce mechanical forces (eg, fluid shear stresses, direct contact forces through collision, acoustic shock waves, and micro-jetting) to the endothelium within the focal zone of the FUS, causing sonoporation of the plasma membrane and disruption of the tight junctions.[31]

Passive cavitation detection (PCD) can provide real-time feedback of acoustic activity. Others have shown success using a PCD feedback system that controls the acoustic pressure to maintain a constant cavitation dose.[32,33] FUS-mediated BBB disruption (BBBD) has been shown in clinical trials to be safe, with no significant neuronal damage, apoptosis, ischemia, or long-term damage to the vessels.[23] Localized BBBD can remain for a period of 3 to 24 h, depending on the intensity of the mechanical stresses modulated through acoustic intensity and MB dose.[34] The safety and reversibility of ultrasound-mediated BBBD and the small volumetric focal zone attainable make FUS/MB a good candidate for targeted drug delivery of molecules, particles, and cells unable to pass the BBB.

We previously identified a strong chemotherapeutic candidate, panobinostat, that has had success against patient-derived xenograft (PDX) DIPG models both in vitro and in vivo.[35,36] Although panobinostat is a small-molecule drug, it binds to albumin protein once injected and is therefore too large to effectively cross the BBB. Our study uses the novel drug delivery method of FUS/MB guided by T2-weighted MRI to deliver panobinostat more effectively to a targeted tumor region and assesses its effectiveness against a patient-derived DIPG tumor model (Figure 1). The BBBD was assessed by T1-weighted MRI pre-/post-gadolinium inject, since most of clinically used gadolinium chelates do not penetrate the intact BBB.

Materials and Methods

Cell Lines and Cell Cultures

DIPG cell line, BT-245[16,37–39] (H3.3K27M-mutant, TP53, pediatric DMG from Dr. Keith Ligon, Dana-Farber Cancer Institute), was biopsied at Boston's Children Hospital. Cells were cultured on plates coated with poly-L-ornithine (0.01%) (Sigma) and laminin (0.01 mg/mL) (Sigma). Cells were grown in Neurocult NS-A media (Stemcell Technologies) supplemented with penicillin-streptomycin (1:100), heparin (2 μg/mL), human epidermal growth factor (EGF; 20 ng/mL), and human basic fibroblast growth factor (FGFb; 10 ng/mL) to maintain all lines.

Cell Viability Assay

Cell proliferation and viability was examined using the MTS [3-(4, 5-dimethylthiazol-2-yl)-5-(3-carboxymethoxyphenyl)-2-(4-sulfophenyl)-2H-tetrazolium] assay. CellTiter 96 AQueous One Solution (Promega) was used. Cells were seeded at 20 000 cells per well into a 96-well plate (Corning) in neurosphere culture, in a media volume of 100 μL. Twenty-four hours later, the cells were treated with a range of doses of panobinostat (Selleckchem) in triplicate. At the end of the drug treatment period (72 h), 20 μL of MTS reagent was added to each well to make a final volume of 120 μL. Absorbance values for plate wells were determined using a BioTek Synergy 2 plate reader at a wavelength of 490 nm. For all tests, the background absorbance was subtracted. IC50 values were determined experimentally through Prism 9.

Microbubble Preparation

Lipid-coated MBs with a perfluorobutane (PFB) gas core were prepared using sonication, as described by Fesitan et al.[40] Under sterile conditions, polydisperse MBs were created and then isolated by differential centrifugation into 3 ± 0.5 μm in diameter. The size isolation process can be found in Supplementary Figure 7. Microbubble concentration and number-/volume-weighted size distributions were measured using a Multisizer 3 (Beckman Coulter). MB concentration (c_i, MBs/μL) versus MB volume (v_i, μL/MB) was plotted, and MB gas volume fraction (ϕMB) was estimated as follows:

$$\phi\text{MB} = \sum_{i=1}^{n} v_i \times c_i$$

where i is the index of the sizing bin, 300 bins (0.7–18 μm). MB preparations were measured 2 h prior to FUS treatment to confirm size and concentration. MBs were stored at 4°C for later use. Microbubbles were diluted to injection concentration within 30 min prior to injection. Supplemental Figure 8 shows MB stability 30 min after dilution.

Orthotopic PDX Mouse Model

All experiments involving animals were conducted according to the regulations and policies of the Institutional Animal Care and Use Committee (IACUC) protocol 00151 in athymic nude mice (nu/nu).

Female mice (Charles River Laboratories) (6–8 weeks old) were initially anesthetized under isoflurane (3.5%). Head was sterilized and a small incision (2 mm) and burr hole (1 mm in diameter) were created at 1 mm right and 0.8 mm posterior to Lambda. ~200 000 BT245-luc2-GFP cells were

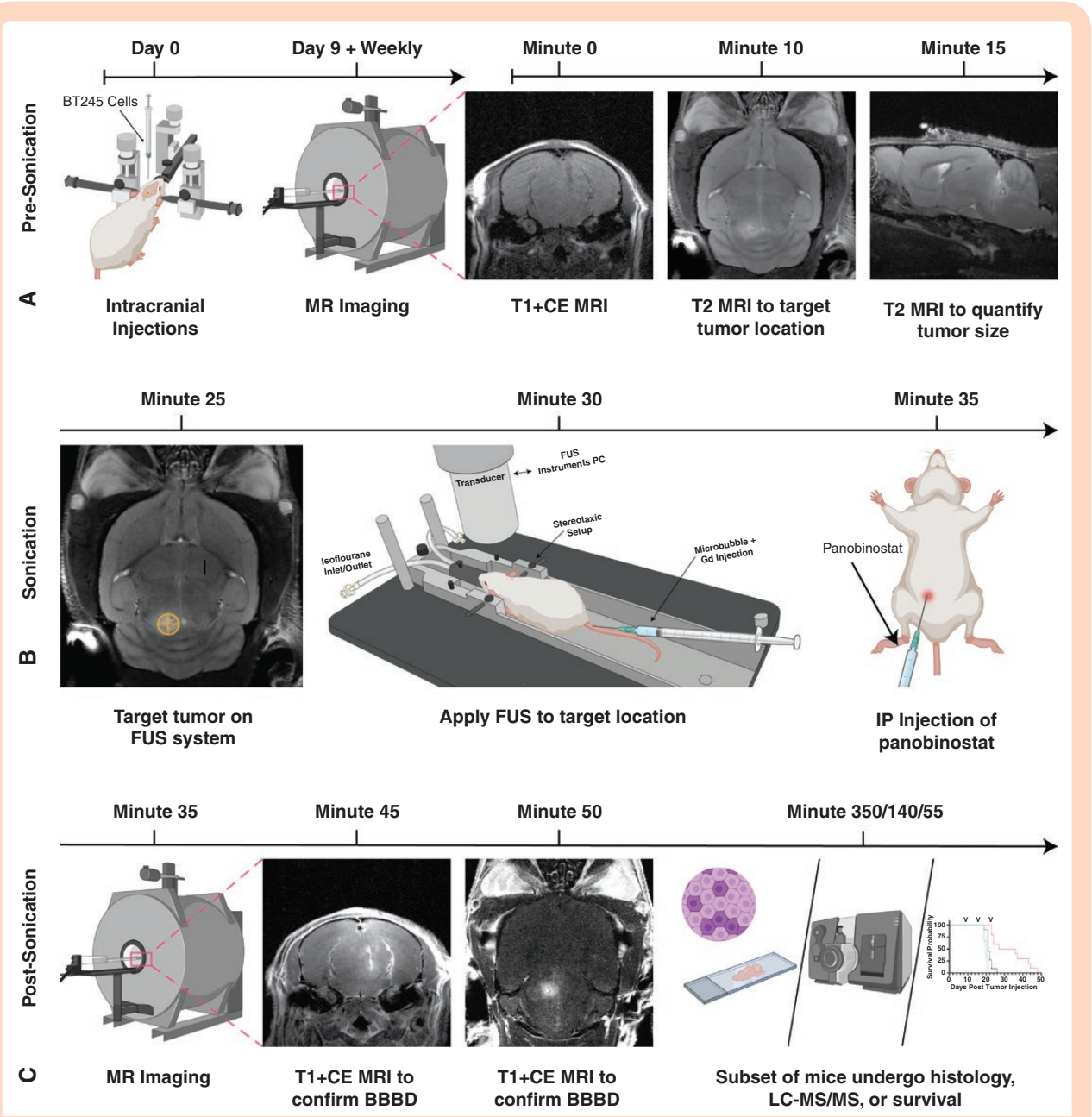

Figure 1. Workflow for our MRI-guided FUS/MB treatments. (A) Prior to FUS treatment, patient-derived BT245 DIPG cells were injected i.c. into the pons region. Mice were placed in MRI and axial T1w images, and coronal and sagittal T2w images were acquired. (B) During FUS treatment, coronal T2w MRI images were used to coregister the FUS targeting system. Mice were then moved from MRI on the same bed to the FUS system, and a water tank was placed on the mouse head with ultrasound gel for acoustic coupling between the animal and ultrasound transducer. Microbubbles and gadolinium (Gd) contrast were injected i.v., the FUS transducer was stereotactically translated to align the acoustic focus to the pons region of the brain guided by the MRI image, and FUS was applied. Directly after FUS treatment, mice were injected with panobinostat i.p. (C) Post-FUS, mice were moved back to the MRI to assess BBB opening by T1w MRI scan of Gd extravasation. Mice were then sacrificed and assessed for histology and drug delivery (LC-MS/MS), or housing to continue survival studies. The timeline of study is shown above all images.

injected at 600 nL/min into the brain 5 mm deep. Mice were given carprofen (5 mg/kg) at 0-/24-/48-h postinjection. Body weight was measured 5 times a week, monitored daily, and euthanized at endpoints (irreversible neurological deficit, body condition score less than 2, or weight loss of greater than 20%). Mouse survival was closely monitored till the end of the experiments. When selecting groups all mice were randomly selected with an even amount used from each cohort of mice deliveries.

Magnetic Resonance Imaging

A Bruker Biospec 9.4 Tesla MR Scanner (Bruker) with a mouse head phase array coil was used for all MR images.

Mice were placed in a modified MRI bed that prevented movement of mouse during transfer from MRI to FUS system. First, a localizer scan was acquired for brain localization. For the FUS treatment group, T1w Multi-Spin-Multi-Echo (MSME) images were acquired in the axial plane (repetition time (TR)/echo time (TE), 720/12 ms; flip angle, 90°; number of averages, 1; field of view, 20 × 20 mm; matrix size, 128 × 128; resolution, 78 × 78 × 700 µm) was performed 12 min after intravenous injection of 0.4 mmol/kg gadobenate dimeglumine (MultiHance). All mice underwent a high-resolution 3D T2-turboRARE scans in sagittal, coronal, and axial planes (TR/TE, 2511/33 ms; flip angle, 90°; number of averages, 4; field of view, 20 × 20 mm; matrix size, 256 × 256; resolution, 78 × 78 × 700 µm). Mice remained on MRI bed and transferred to FUS system for treatment, where an intravenous injection of 0.1 mL gadobenate dimeglumine (MultiHance) was given. After treatment, mice were moved back to MRI and a post-FUS T1-weighted sequence was acquired after 12 min post-gadobenate dimeglumine injection.

MR Image Analysis

T1-weighted images were used to quantify extent of BBB disruption using FIJI. First, a region of interest was defined within contralateral side of the brain (left) in order to determine the baseline intensity. The area of BBBD was defined by the control region plus 2 SD. The area and volume were calculated on all MRI slices. The contrast enhancement was determined by average intensity within BBBD volume and dividing it by the intensity of the control region. T2-weighted MR images were used to calculate tumor volumes. Three-axis images were uploaded to Slicer.[41] Tumor margins were defined on each slice and a total volume was calculated by summing each slice volume and multiplying by slice thickness (0.7 mm). This was completed on both sagittal, and axial slices and the average volume was taken.

MRIgFUS and Drug Treatment

After 9 days weekly treatments of panobinostat (10 mg/kg) began and continued for 3 weeks. Experimental set-up is shown in Figure 1B. A single-element, focused transducer (frequency: 1.515 MHz, diameter: 30 mm) was driven by the RK-50 system (FUS Instruments, Supplementary Figure 9). A single-element, focused transducer (frequency: 0.7575 MHz, diameter: 10 mm) was used for PCD. Using the T2-weighted MR image (coronal), the tumor center was targeted (Figure 1A). Ultrasound gel was placed on the mouse head without air bubbles. An acoustically transparent tank filled with degassed water was placed on top of the gel Figure 1B. Microbubbles (25 µL/kg; 0.1 mL) and 0.1 mL of MultiHance were injected intravenously through a tail vein injection via 26 Ga needle. Just prior (10–20 s) to injection, FUS was applied to determine baseline acoustic response. FUS parameters were as follows: 10-ms PL, 1 Hz PRF, 180 s treatment time, and a PNP of 0.615 MPa. Voltage data from the PCD was collected during the entire FUS treatment and analyzed as previously described.[30] Remaining PCD analysis was done using MATLAB including the calculations of harmonic and broadband cavitation doses (BCDs). Directly after FUS treatment, panobinostat (10 mg/kg; diluted in 0.125 mL solution of 4% DMSO, 46% PEG300, and 50% PBS) was injected intraperitoneally. Mice were then sent back to MRI to complete post-FUS T1w imaging. Groups were set to FUS/MB + panobinostat (n = 10), panobinostat alone (n = 10), and control (n = 3). FUS/MB was not included given the lack of evidence, FUS/MB alone showed a significant survival benefit.[42,43]

Liquid Chromatography-Tandem Mass Spectrometry (LC-MS/MS)

A subset of mice (n = 18) was kept for 16 days post-BT245 cell injections. Six mice were treated with FUS/MB and panobinostat, 6 were treated only with panobinostat, the final group (6) was untreated. At 60 min post-panobinostat administration, blood samples were collected via cardiac puncture. Immediately after, a transcardial perfusion with PBS was conducted. The brain was extracted, dissected, and snap frozen (Figure 4E). Blood was allowed to clot for 45 min then centrifuged at 2000×g for 15 min. Serum was collected and snap frozen. All tissues were stored at –80°C until LC-MS/MS analysis. Samples were analyzed by the School of Pharmacy. The analysis was performed on an Applied Biosystems Sciex 4000 (Applied Biosystems) equipped with a Shimadzu HPLC (Shimadzu Scientific Instruments, Inc.) and Shimadzu auto-sampler. An extend-C18 Zorbax column (Agilent Technologies) 4.6 × 50 mm, with a column guard held at 40°C was utilized. Solvent A: HPLC H_2O with 10 mM NH_4OAc and 0.1% formic acid; and solvent B: 1:1 methanol:acetonitrile. In triplicate, a 16-point standard curve of panobinostat was prepared starting from 20.0 µM and serially diluted. Samples were transferred to a 96-well plate and analyzed by LC/MS-MS method; 40 µL sample sizes were injected onto the column.

Immunohistochemistry and Histology

A subset of mice (n = 7) underwent histological analysis. Tumors were allowed to grow for 16 days and treated with FUS/panobinostat (n = 3), or panobinostat only (n = 3). A final mouse was analyzed after 3 weeks of tumor growth without any treatments. Six hours after treatment (if applicable), mice were sacrificed and perfused with 10% formalin (Thermo Fisher Scientific) for 3 min. Brains were immediately dissected and put into 10% formalin solution overnight. Primary antibody staining was done with anti-Ki-67 1:100 (ab15580, Abcam), and samples were incubated overnight at 4°C. Signals were detected using DAB stain and counterstained with hematoxylin. Microscope slides were imaged on a brightfield microscope at 1 to 50×. Quantification of images was done at FIJI (NIH), where a color deconvolution was used for DAB and hematoxylin staining. Each deconvolution image was converted to binary, where a threshold was determined to differentiate all cells in the image. The Analyze Particles function was used

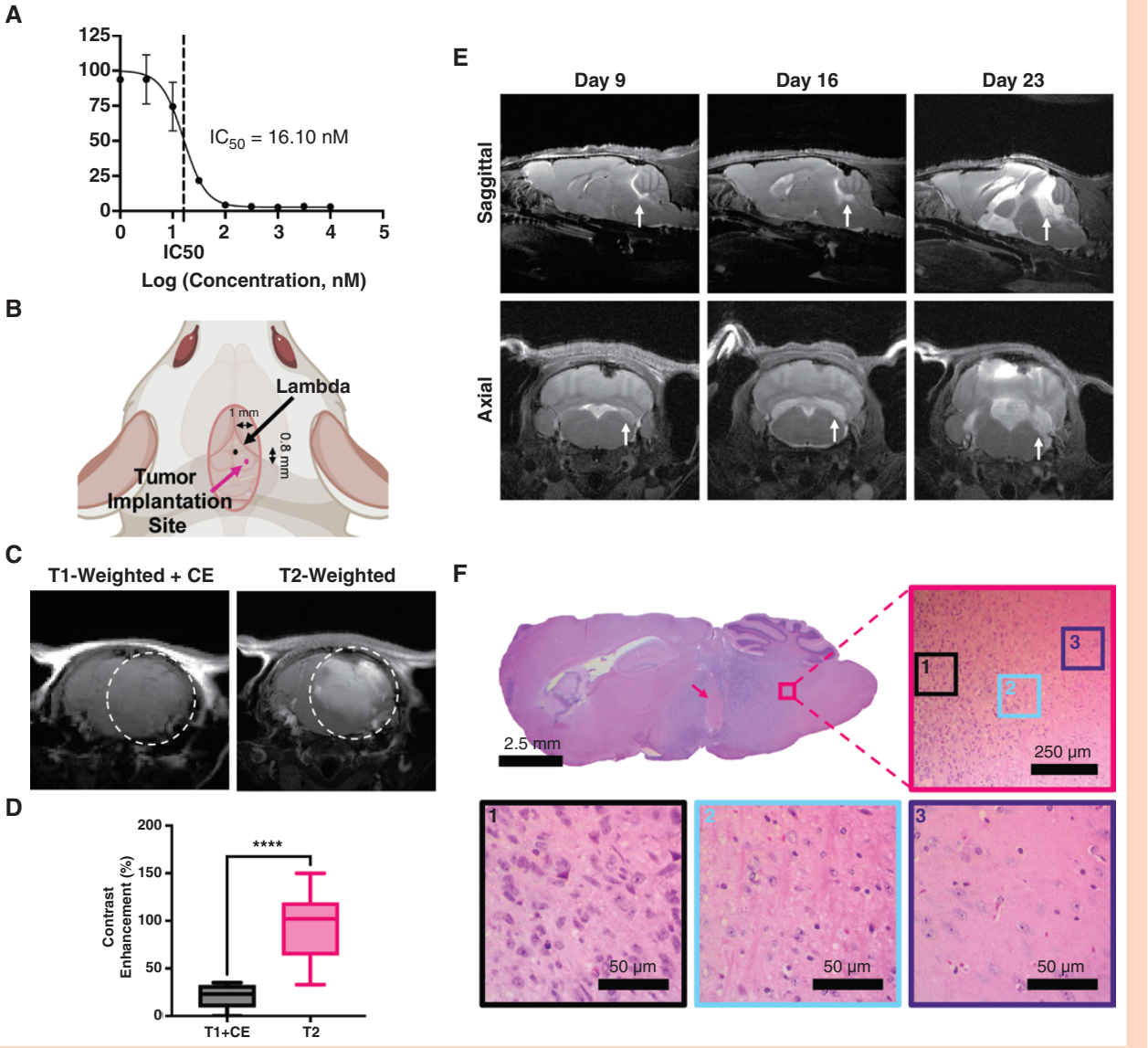

Figure 2. Diffuse intrinsic pontine glioma BT245 PDX model. (A) Cell viability of BT245 cells treated with panobinostat for 72 h assessed by MTS assay. Vertical dotted line represents IC_{50}. Values represent the mean ± standard deviation (n = 3). (B) Cartoon of tumor implantation site with respect to Lambda skull landmark. (C) T1w contrast-enhanced (CE) MR image (left) prior to FUS/MB showing little tumor enhancement in the T2w MR detectable tumor (right). (D) Quantification of contrast enhancement between the 2 MRI imaging modes (n = 9). (E) T2w MR images at 9, 16, and 23 days post-tumor implantation in the control group. Images show intrusive tumors at the pontine region with growth that progresses to the ventricles and adjacent brain structures. (F) Histological analysis of tumor at 3 weeks post-tumor implantation. Full view of H&E staining shows whole tumor region, with pink arrow illustrating region of necrosis. Figure is zoomed in to a region on the border of tumor (pink border) and healthy tissue. Also shown are zoomed regions of the tumor (black border), margin (blue border), and healthy tissue (purple border). Abbreviations: MR = magnetic resonance; T1w = T1-weighted; T2w = T2-weighted; H&E = hematoxylin and eosin. IC_{50} = half-maximal inhibitory concentration.

to count cells. Each slice was analyzed in 3 separate FOV within the region.

Statistical Analysis

All data collected are presented as mean ± SD. No preprocessing was done to data with the exception of voltage data collected from the PCD. PCD data were preprocessed as described in Martinez et al.[30] All statistical analysis was completed in Prism 9 (GraphPad). Star representations of P-values are indicated in captions and less than .05 was indicative of statistical significance. An unpaired Student's t test and Kaplan-Meier estimates were used to compare 2 groups and survival analysis, respectively.

Results

BT245 Xenograft Mouse Models Represent DIPG and DMGs

Among current clinically approved chemotherapeutics, panobinostat was selected for this study as the most effective drug in vitro for our patient-derived DIPG cells. To confirm efficacy of panobinostat, BT245 DIPG cells were put through dose escalation trials and MTS assay to determine the half-maximal inhibitory concentrations (IC_{50}). The resulting IC_{50} value for panobinostat was 16.1 nM (Figure 2A). Panobinostat was chosen because it had the lowest IC_{50} of the 4 drugs we tested (Selinexor, Riboclib, and Paxalib, Supplementary Figure 1). Panobinostat also shows poor BBB penetrance. Most (~90%) of panobinostat, which associates with albumin via hydrophobic intermolecular forces,[44] is protein bound in blood and prevents its penetration across the BBB or BBTB.[35,45]

Our PDX orthographic mouse model was established by implanting 2×10^5 luciferase-expressing BT245 cells into the pons of nude athymic mice (Figure 2B). This cell line has been used extensively in murine models (Supplementary Table 2).[16,39,46] Tumor progression was monitored using bioluminescent imaging for the first week (Supplementary Figure 2). Thereafter, MRI was used to monitor tumor volumes, guide, and validate FUS treatments. One important component of this murine model is the lack of contrast enhancement on T1-weighted (T1w) MR images owing to poor BBB penetration of the gadobenate dimeglumine contrast (Figure 2C and D), making this model more clinically relevant than those with leaky tumors. T2-weighted (T2w) MRI is the basic of all clinical diagnostic scans for DIPG patients and was employed in this study to determine the exact tumor location and volumes (Figure 2C and D). The first control (no treatment) group showed a significant tumor progression (Figure 2E). Our xenograft model showed a clinically relevant growth pattern marked by the ability to migrate through the cerebral spinal fluid and metastasize elsewhere in the central nervous system (Figure 2E, Supplementary Figure 3). H&E staining illustrated the focal region of growth with a diffuse tumor margin. After long periods of tumor growth, areas within the mass began to show regions of necrosis, most pronounced at the tumor center (pink arrow, Figures 2F and 4F).

Microbubbles Are Monodispersed in Size and Concentration

After the size isolation of 3 μm-diameter microbubbles, the MB formulation was inspected using brightfield microscopy as shown in Figure 3A. The monodispersity of microbubbles was illustrated with narrow peaks for both number- and volume-weighted distributions (Figure 3B). The resulting mean diameters were 2.8 and 3.2 μm, respectively. Each population was individually analyzed to confirm consistent microbubble volume dose injected. Figure 3C illustrates the microbubble concentration versus volume plot integrated to determine the gas volume fraction (ϕMB). The mean ϕMB for 1010 MBs/mL was 13.5 μL/mL (Supplementary Table 1).

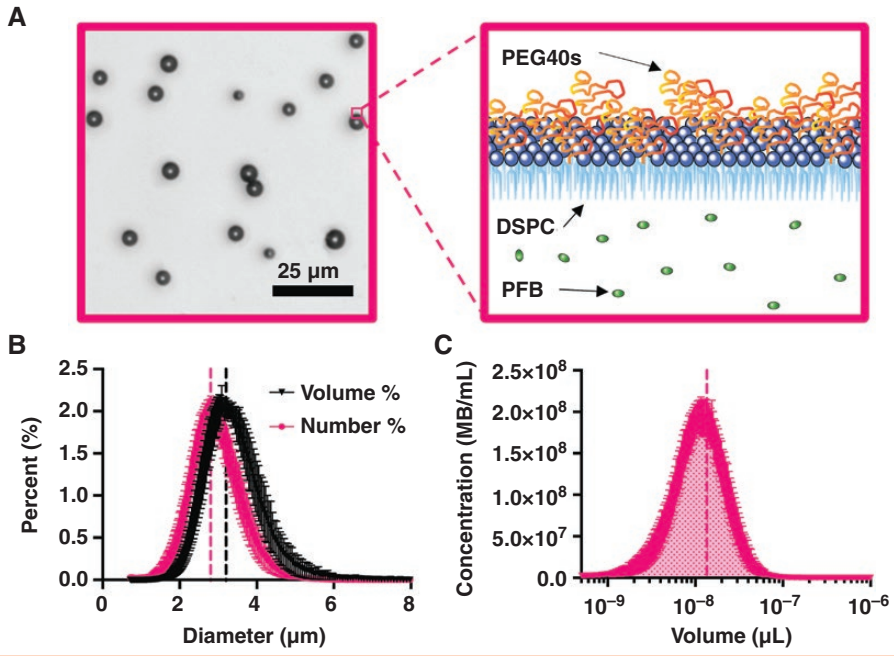

Figure 3. Microbubble characterization. (A) Brightfield image of 3 μm-diameter microbubbles (left). Cartoon of microbubble structure showing lipid, PEG brush, and internal gas (right). (B) Number- and volume-weighted size distributions. (C) Microbubble concentration against microbubble volume at a basis concentration of 1010 MBs/mL; shaded area under the curve represents the gas volume fraction. Vertical dotted lines represent mean values for both B and C. Data points represent the mean ± standard deviation ($n = 8$). Abbreviations: PEG = polyethylene glycol; PEG40s = PEG_{40} stearate; DSPC = distearoylphosphatidylcholine; PFB = perfluorobutane; MB = microbubble.

MRI-Guided FUS/MB Improves Tumor Uptake of Panobinostat at Target Site

Accurate and precise BBB opening at the target site was confirmed for our conditions by MRI. Figure 4A illustrates the contrast enhancement of MultiHance in the brain parenchyma owing to BBB disruption by FUS/MB. Similar to our drug, panobinostat, this Gd contrast agent weakly binds to albumin and exhibits similar BBB penetration.[45,47] We saw no extravasation just prior to FUS/MB treatment, then a significant amount just after the application of FUS/MB. Images taken just prior to FUS/MB application the following week also showed no Gd extravasation, confirming closure of the BBB after the prior FUS/MB treatment. A subset of mice was injected with Evan's blue dye. Figure 4B illustrates dye extravasation (bottom) compared to the MultiHance extravasation (top), showing targeting and patterning to T1w CE images. Histological analysis was performed on a FUS/MB-treated mouse to confirm the lack of morphological damage (Figure 4C). H&E staining showed no major changes other than small amounts of red blood cell extravasation at the bottom of the FUS focal zone. After each treatment, mice remained within 94% of their initial body weight at 7 days post-FUS/MB treatment (Figure 4D).

Once we confirmed BBB disruption was safe and effective at delivering MultiHance, we next confirmed targeted panobinostat delivery to the tumor. At 2 weeks post-tumor injection, mice were treated with MRI-guided FUS/MB immediately followed by i.p. injection of panobinostat (10 mg/kg). Liquid chromatography with tandem mass spectrometry (LC-MS/MS) was used to determine the concentration of panobinostat in the tumor region and front part of the cortex. FUS/MB was associated with significantly more panobinostat in the tumor region (194.3 ng/g) than in the frontal cortex region (65.6 ng/g, Figure 4F). Mice showed significantly more panobinostat in the tumor region than when treated with FUS/MB than without FUS/MB, with a mean concentration of 194.3 versus 61.8 ng/g ($P < .0001$, Figure 4F). The tumor-to-serum ratio showed a significant increase between FUS/MB and non-FUS/MB mice, with a mean of 0.74 versus 0.18 mL/g ($P < .05$, Figure 4G). Control mice treated with FUS/MB but without panobinostat showed no concentration of panobinostat in either the blood or brain tissue (Supplementary Figure 4).

Prior to all treatments, T1w CE MR images were taken and analyzed for the extent of BBB opening volume and total contrast enhancement. The resulting BBB opening volumes were found to be 8.74, 9.68, and 10.56 mm^3 as the weeks progressed (1, 2, and 3 respectively). Contrast enhancements for each were 51.5%, 63.1%, and 85%, respectively. No significant difference was observed in either volume or contrast enhancement during treatments week to week (Figure 4H and I).

Mild Harmonic MB Activity During FUS Confirmed by PCD

During each FUS/MB treatment, a passive cavitation detector (PCD) recorded the acoustic response within the focal region. All voltage-vs-time signals were preprocessed (Figure 5A) then converted to the frequency domain for analysis (Figure 5B). As expected, during treatments there was a strong harmonic response absent of significant broadband feedback, indicating mild MB harmonic oscillations without inertial implosions (Figure 5C). During the initial time just after the injection of MBs, we saw a spike in harmonic cavitation dose (HCD, Figure 5D). As FUS continued, there was a decay curve as microbubbles were cleared from circulation. Meanwhile, BCD maintained a similar intensity before and after microbubble injection, indicative of general system noise. Figure 5E shows the spectral content of a single 10-ms pulse with 0.5 ms readings before and after FUS. Beyond the fundamental frequency response, significant sub- and ultraharmonics signals were observed only during treatment. These single pulses were connected (without 0.5 ms ends) to give an overall visualization of the treatment, showing that the sub- and ultraharmonic components were maintained during the entire FUS treatment (Figure 5F).

FUS/MB and Panobinostat Is Effective at Reducing Tumor Growth and Improving Survival

Our data confirmed increased panobinostat delivery and its tumor cell cytotoxic effectiveness against DIPG in our murine model. During each treatment, three-dimensional (3D)-T2w MR images in axial, coronal, and sagittal planes were acquired to monitor tumor volumes (Figure 6D). MR images were analyzed to find total tumor volume and monitor it from week to week (Figure 6B) and showed that FUS/MB and panobinostat treatment inhibited tumor growth. MRI also showed significant intracranial edema, ventricle infiltration, and inflammation at later time points. Tumor progression was significantly different between treated and untreated groups by week 3, where mean volume was 49.7 mm^3 for non-FUS/MB and 14.1 mm^3 for FUS/MB-treated mice ($P < .01$). Neither group showed a significant drop in weight until week 3, when non-FUS/MB mice dropped to 88% of the starting weight. FUS/MB-treated mice weight dropped to 91% of the starting weight, at most (Figure 6A). All FUS/MB mice weights are shown at actual values in Supplemental Figure 5. Kaplan-Meier survival curves showed an increase in survival for the FUS/MB and panobinostat group with a mean survival of 31.5 days. This was compared to the non-FUS/MB with panobinostat control group, which had a mean survival of 21 days (Figure 6C). Immunohistochemical analysis of both treatment arms was conducted after a single treatment. Results showed that Ki-67-positive cells had decreased significantly in the FUS/MB-treated group (Figure 6E). P53 was also stained and showed no significant difference in percent of positive cells (Supplemental Figure 6). Representative images are shown on the left side of Figure 6E, and quantitative analysis is shown on the plot on the right.

Discussion

While outcomes have improved for almost all childhood cancers, DIPG has shown little to no improvement in survival over decades. The tumor's diffuse nature and location

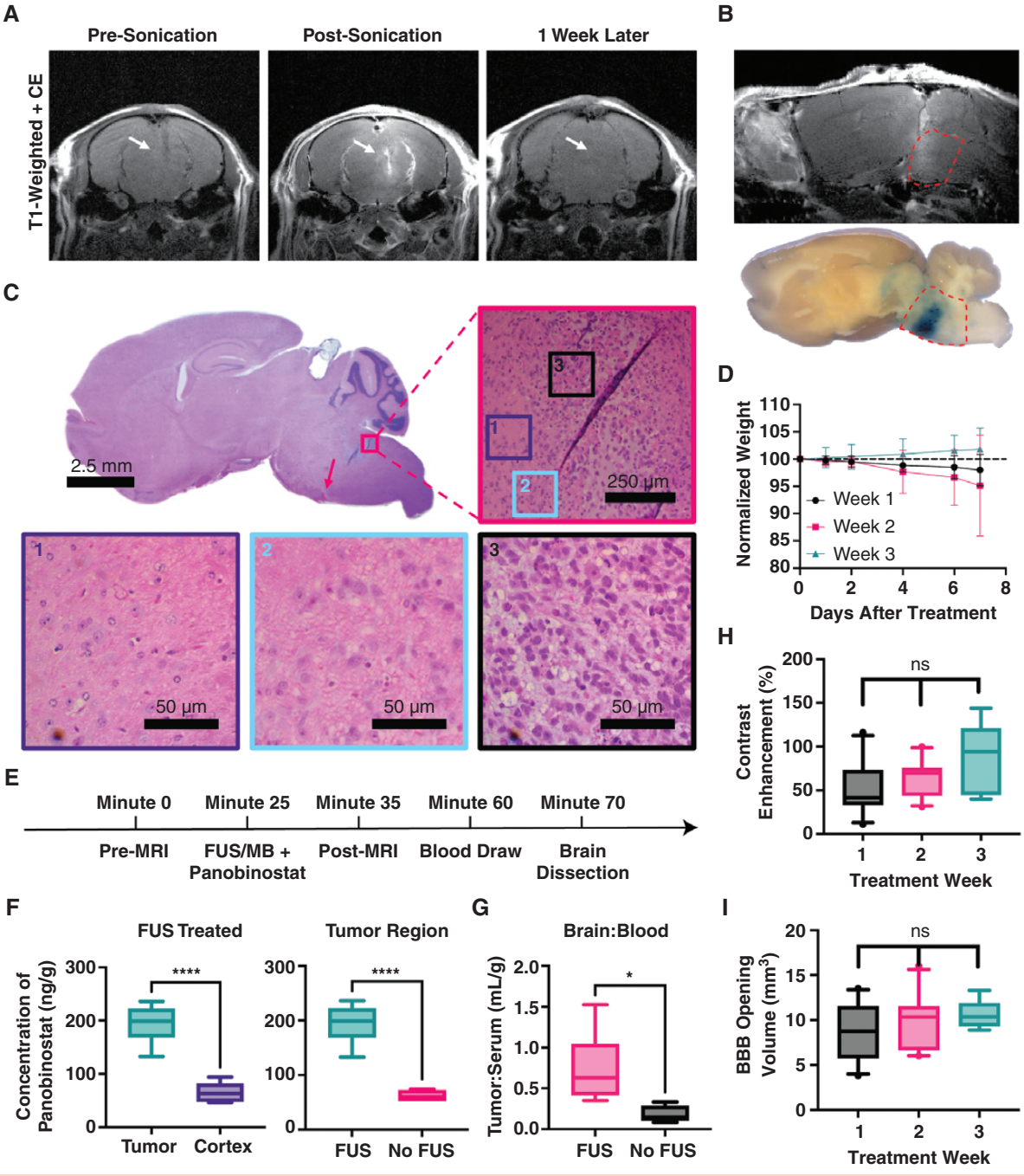

Figure 4. Confirmation of BBB opening and increased delivery of panobinostat into DIPG tumors using MRI-guided FUS/MB at target region. (A) T1w CE MR images just before FUS/MB treatment (left), directly after treatment (center) showing BBB opening as bright spots owing to Gd extravasation and 1 week post-FUS treatment (right) showing closing (white arrows); all images are in the axial plane. (B) Confirmation of BBB opening in the sagittal plane by T1w MRI (top), and Evan's blue dye (bottom). Pontine region outlined in red dotted line. (C) H&E staining of the whole brain, with a pink arrow illustrating the region of red blood cell extravasation. Figure is zoomed (50×) into the region on the border of tumor (pink) and healthy tissue. Also shown are zoomed-in regions of healthy tissue (purple border), tumor margin (blue border) and tumor (black border). (D) Plot showing the normalized body weight of each mouse after treatments. Data are split between weeks. There is no significant difference between each week. (E) Timeline of blood and brain sample collection. (F) LC-MS/MS results showing panobinostat concentration after MB+FUS treatment in the tumor region vs. cortex (left). Concentration difference between both tumor regions of FUS/MB-treated and untreated mice (right). (G) The tumor-to-serum ratio of panobinostat concentration for FUS/MB versus MBs alone (no FUS). (H) Contrast enhancement within the treated tumor region compared to the contralateral side. (I) Volume of BBB disruption determined by MRI T1w CE. Data represent mean ± standard deviation (n = 6 for A–C; n = 25 for D and E). Symbols *, **** represent $P < .05$ and $P < .0001$, respectively.

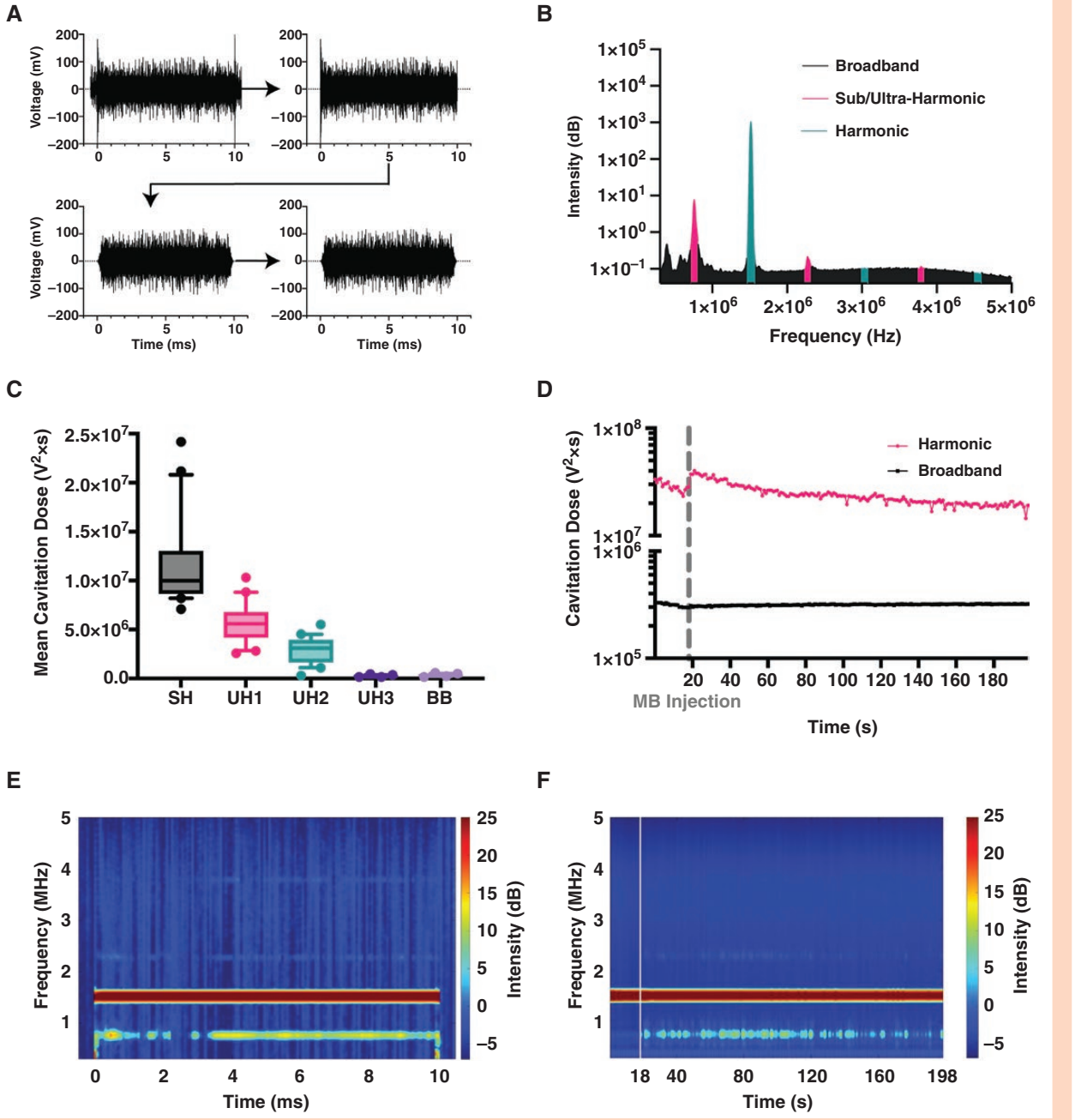

Figure 5. Passive cavitation detection of microbubble activity. (A) Voltage data preprocessing including cropping, Tukey windowing, then low-pass filtering. (B) PCD voltage plot showing the area under the curve for sub/ultraharmonics, harmonics, and broadband peaks. (C) Normalized mean cavitation doses found at each area of interest including sub-harmonic, first, second, and third ultraharmonic, and broadband (SH, UH1, UH2, UH3, BB, respectively). Data represent mean ± standard deviation (n = 20). (D) Cavitation doses calculated at each FUS pulse and plotted over the entire FUS treatment. A break in the ordinate was made to better view both curves. Each point represents the mean (n = 20). (E) Representative spectrogram of single 10-ms pulse with 0.5 ms recording before and after. (F) Representative spectrogram of a whole treatment where each 10-ms pulse is shown for each second (1 Hz pulse repetition frequency). Time in between FUS pulses is not shown. Vertical line represents the time when microbubbles were injected.

make it to be unresectable and limit any ablation options.[1] Given the retention of the BBB in DIPG, drug delivery has another hurdle.[48] This is evident on MRI, in which contrast-enhanced images show little to no enhancement.[2] Many therapeutics have shown effectiveness in vitro; they just cannot pass the BBB in effective enough doses to treat the cancer without causing systemic toxicity.[48]

MRI-guided FUS with microbubbles (FUS/MB) has become a noninvasive way to temporarily disrupt the BBB, providing a window for therapeutics to enter only at the

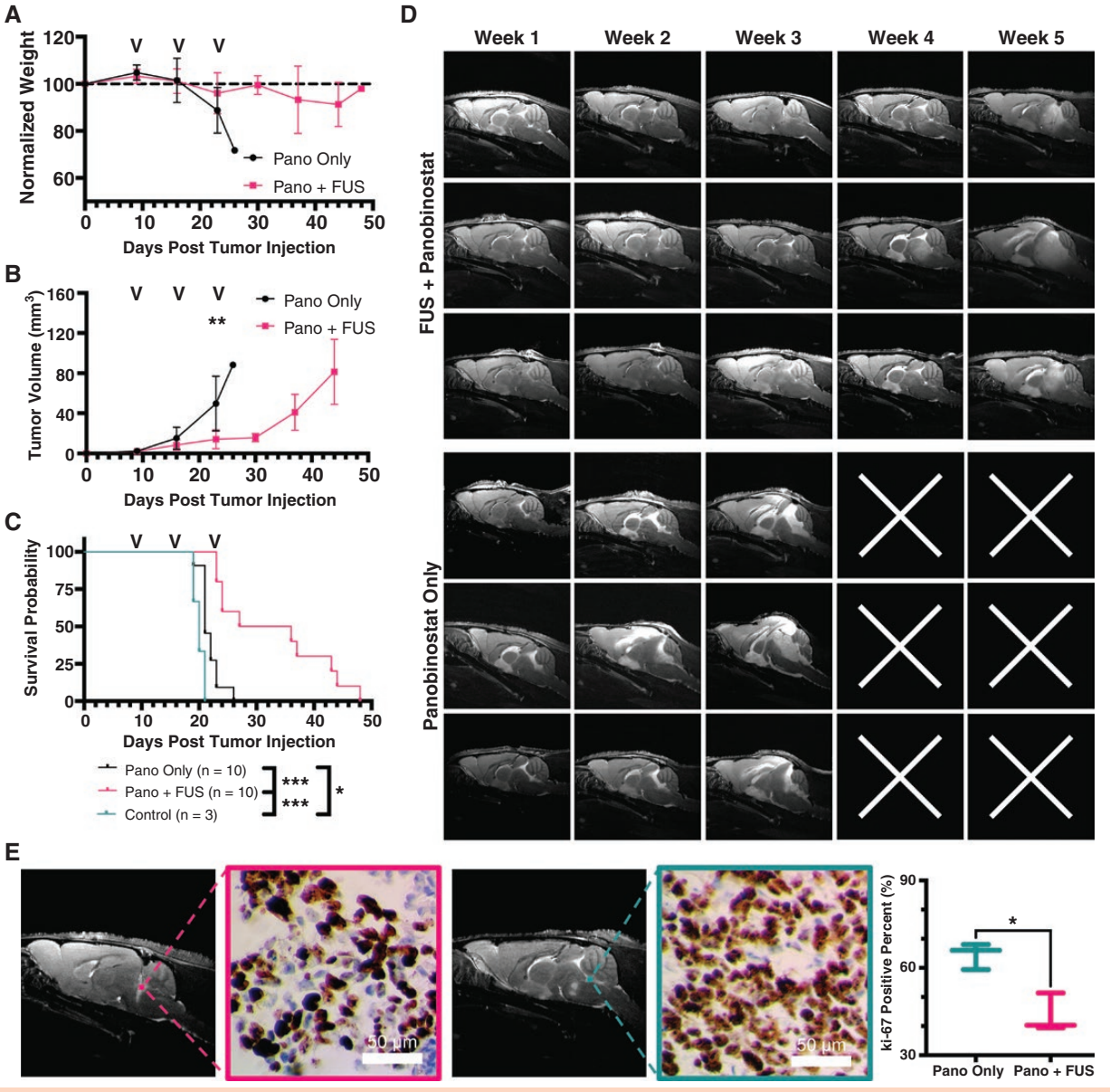

Figure 6. Focused ultrasound (FUS)/microbubbles (MB) with panobinostat reduces tumor growth and improves survival. (A) Longitudinal study of mouse body weight obtained weekly, (B) tumor volume using T2w MRI, and (C) KP survival curves. Black arrows on plots represent the treatment days. (D) Representative T2w MRI (sagittal axis) images of tumor progression for 3 representative mice in each group. Top 3 rows show MB + FUS with panobinostat-treated mice, and bottom rows are only panobinostat (no MB + FUS). White "x" illustrates the death of the mouse prior to the MR imaging that week. (E) Representative images of Ki-67 staining and its relation to MR images (left) and quantification of Ki-67 positive cells in tumor region for panobinostat + MB + FUS and panobinostat only (right). Significance testing was done using an unpaired Student's *t* test for B ($n = 10$) and E ($n = 3$), and Mantel-Cox test for C ($n = 10$), where *, **, *** indicate $P < .05$, $P < .01$, and $P < .001$, respectively.

tumor site. Focused ultrasound transducers can maintain a focal region on a millimeter scale and therefore can hit accurately and precisely only where the tumor is located. Several groups have looked into this technology to deliver drugs to solid tumors. Some of these trials have shown increased survival and reduced tumor growth.[32,42,49–53] As a consequence, this technology has been translated into clinical trials showing the safety of FUS/MB treatments, and current clinical trials are focused on efficacy with tumor types other than DIPG, including glioblastomas. Due to the depth and targeting complexity of the brainstem, only a few groups have investigated using this technology for pontine DMG.[42,52,54,55] Over the last 5 years, 2 groups have looked into using FUS/MB to treat DMGs. Initially, in 2018, Alli et al. showed the ability to deliver doxorubicin to the pons without any neurological issues. Later, Englander et al. used etoposide and treated for 2 consecutive weeks, confirming the safety of multiple treatments. To our knowledge, no group has yet shown a significant increase in survival for DMGs.[42,52,54]

In our study, we used a H327-altered, TP53-mutant DIPG PDX murine model to determine the efficacy and safety of MRI-guided FUS/MB treatments. We tested the HDAC inhibitor, panobinostat, due to previous drug screening studies using patient-derived DIPG cell lines.[9] Panobinostat specifically targets H3K27M cell populations, showing antitumor efficacy both in vitro and in xenograft models.[56] Overall, these studies showed impaired cell proliferation and viability of DIPG cells.[9] In cell lines with the H3K27M alteration, panobinostat reduced tumor growth and increased H3K27 trimethylation. While Hennika et al. saw epigenetic effects, unfortunately the systemic doses (20 mg/kg) resulted in significant toxicity. When the dose was reduced (10 mg/kg), it was well tolerated but failed to prolong survival.[36] Unlike our model, many of these prior models showed a slightly leaky BBB.[36] The molecular weight of panobinostat is relatively small (439.51 Da for the base form of panobinostat and 349.43 Da for the anhydrous lactate form),[45] but most (~90%) of the drug is protein bound in blood, which prevents its penetration across the BBB or BBTB.[35] As we showed, our cell line yields an intact BBB, which is more clinically relevant. Our objective was to use MRI-guided FUS/MB to obtain high enough doses at the tumor site while minimizing toxic side effects by injecting the lower dose (10 mg/kg). Using MR-guided FUS/MB, we demonstrated a significant increase in panobinostat concentration in the parenchyma at the tumor location compared to the cortex (3-fold), illustrating both the delivery enhancement, and targeting capability of the technology. We also found a significant increase in panobinostat in FUS/MB-exposed tumors over non-FUS/MB ones (over 3-fold). With similar serum values between groups, this led to a 4-fold increase in tumor-to-serum ratio at 1 h post-i.p. panobinostat injection.

Our study is the first to demonstrate 3 repeated treatments to the brainstem. Similar to Englander et al., we saw reopening with repeated treatments.[52] We consistently had a BBB opening volume of ~10 mm^3 over all 3 weeks, which is just above the expected focal volume of the transducer (~8.4 mm^3). The volumes did not change significantly over the 3 weeks of treatment. Many research groups have begun to use PCD feedback to ensure a mild and consistent cavitation dose.[32,57,58] Our study used a constant MI (0.4) with a bolus injection of monodisperse microbubbles. Our PCD recording prior to microbubble injection showed the spike in harmonic oscillations as microbubbles entered circulation, and the HCD decreased with subsequent clearance following the expected decay from prior pharmacokinetic analysis of similarly formulated and sized microbubbles.[59] The use of a PCD feedback treatment plan necessitates a continuous infusion of MBs, and hence was considered too time-consuming for our purposes. The harmonic acoustic response is known to be associated with mild MB oscillations,[31] which are also known to be effective for BBB opening. We also avoided the broadband (inertial) acoustic response associated with MB implosions and unwanted biological effects.[31,60]

Despite encouraging results of the FUS/MB technique in glioblastomas, a survival benefit with FUS/MB had not yet been shown in animal models of DMG. Here, we demonstrate the first significant survival benefit in a DIPG model using FUS/MB. We also show that FUS/MB-mediated BBB opening is accurate, precise, and reproducible in weekly treatments. Normalized body weight showed relatively stable weight for the FUS/MB-treated mice. During the initial 4 weeks of the study, we found significantly decreased tumor growth in the FUS/MB-treated mice, showing the emergent potency of an otherwise ineffective anticancer drug by use of a noninvasive image-guided drug delivery technology. It is likely that the reduced tumor growth we observed was responsible for the survival benefit, in which we observed an increase in the average overall survival from 21 to 31.5 days for the FUS/MB-treated mice versus drug alone.

Our murine PDX model shows similar pathology, mutations, MRI features, and growth patterns to DIPG in human patients. The MRI-guided FUS/MB technology was shown here to be a safe and effective way to provide a higher concentration of panobinostat at the tumor region without increasing systemic dose or off-target effects. However, our study had some limitations. Our study was designed to confirm the safety and effectiveness of FUS/MB for only 4 weeks. Specifically, it must be investigated whether or not these DMG tumors can develop a resistance to panobinostat and/or FUS/MB over time. Other research with panobinostat would indicate that the former may occur. Finally, our exact drug formulation (free panobinostat) would have to change as it is no longer on the market. We would move to the water-soluble formulation (MTX-110) currently being used in conjunction with CED. Moreover, our work here is generalizable to other key drugs.

In conclusion, our group has shown that MR-guided FUS/MB is a noninvasive, safe, and effective way to temporarily disrupt the BBB and increase drug delivery of panobinostat in a clinically relevant DIPG orthotopic xenograft mouse model. We showed the potential to treat this model weekly for 3 weeks while maintaining safe and similar BBB opening volumes. Using more stringent control over microbubble size and volume dosage was shown to be safe and effective leading to the first ever survival benefit of a DMG model using FUS/MB. This is a critical preclinical step to use this technology for DIPG patients in human clinical trials.[61,62]

Supplementary material

Supplementary material is available online at *Neuro-Oncology Advances* online.

Keywords

blood–brain barrier opening | diffuse midline gliomas | focused ultrasound | drug delivery | microbubbles

Funding

Funding for this work was provided by the Colorado Cancer League (212811-AG to M.B., A.G., N.S.), the National Science Foundation (DGE 2040434 to P.M.) and the National Institutes of Health (R01 CA239465 to M.B.).

Acknowledgments

The authors would like to thank John Desisto for his expertise throughout this project. Parts of Figures 1 and 2 were made using Biorender.com.

Conflict of interest statement

The authors declare that they have no competing interests.

Authorship statement

Conceptualization: N.S., A.G., M.B. Methodology: P.M., G.N., J.S., M.F.W., A.P., J.J.S., K.H.S., N.E., N.S., A.G. Investigation: P.M., G.N., J.S., A.P., B.B., M.S., A.M., J.J.S., N.S. Visualization: P.M., G.N., J.S., J.J.S., N.S. Funding acquisition: N.S., A.G., M.B. Project administration: N.S., A.G., M.B. Supervision: N.S., A.G., M.B. Writing—original draft: P.M. Writing—review and editing: N.E., N.S., A.G., M.B.

Data and materials availability

All data are available in the main text or the supplementary materials.

References

1. Vitanza NA, Monje M. Diffuse intrinsic pontine glioma: from diagnosis to next-generation clinical trials. *Curr Treat Options Neurol.* 2019;21(37):37–11.
2. Leach JL, Roebker J, Schafer A, et al. MR imaging features of diffuse intrinsic pontine glioma and relationship to overall survival: report from the international DIPG registry. *Neuro Oncol.* 2020;22(11):1647–1657.
3. St. Jude Children's Research Hospital–Washington University Pediatric Cancer Genome Project. Somatic histone H3 alterations in pediatric diffuse intrinsic pontine gliomas and non-brainstem glioblastomas. *Nat Genet.* 2012;44(3):251–253.
4. Louis DN, Perry A, Wesseling P, et al. The 2021 WHO classification of tumors of the central nervous system: a summary. *Neuro Oncol.* 2021;23(8):1231–1251.
5. Antin C, Tauziède-Espariat A, Debily M-A, et al. EZHIP is a specific diagnostic biomarker for posterior fossa ependymomas, group PFA and diffuse midline gliomas H3-WT with EZHIP overexpression. *Acta Neuropathol Commun.* 2020;8(183):183.
6. Findlay IJ, De Iuliis GN, Duchatel RJ, et al. Pharmaco-proteogenomic profiling of pediatric diffuse midline glioma to inform future treatment strategies. *Oncogene.* 2022;41(4):461–475.
7. Mohammad F, Weissmann S, Leblanc B, et al. EZH2 is a potential therapeutic target for H3K27M-mutant pediatric gliomas. *Nat Med.* 2017;23(4):483–492.
8. Chan K-M, Fang D, Gan H, et al. The histone H3.3K27M mutation in pediatric glioma reprograms H3K27 methylation and gene expression. *Genes Dev.* 2013;27(9):985–990.
9. Grasso CS, Tang Y, Truffaux N, et al. Functionally defined therapeutic targets in diffuse intrinsic pontine glioma. *Nat Med.* 2015;21(6):555–559.
10. Hashizume R, Andor N, Ihara Y, et al. Pharmacologic inhibition of histone demethylation as a therapy for pediatric brainstem glioma. *Nat Med.* 2014;20(12):1394–1396.
11. Vitanza NA, Biery MC, Myers C, et al. Optimal therapeutic targeting by HDAC inhibition in biopsy-derived treatment-naïve diffuse midline glioma models. *Neuro Oncol.* 2021;23(3):376–386.
12. Lin GL, Nagaraja S, Filbin MG, et al. Non-inflammatory tumor microenvironment of diffuse intrinsic pontine glioma. *Acta Neuropathol Commun.* 2018;6(51):51.
13. Ross JL, Chen Z, Herting CJ, et al. Platelet-derived growth factor beta is a potent inflammatory driver in paediatric high-grade glioma. *Brain.* 2021;144(1):53–69.
14. McCully CM, Pastakia D, Bacher J, et al. Model for concomitant microdialysis sampling of the pons and cerebral cortex in rhesus macaques (*Macaca mulatta*). *Comp Med.* 2013;63(4):355–360.
15. Warren KE. Beyond the blood:brain barrier: the importance of central nervous system (CNS) pharmacokinetics for the treatment of CNS tumors, including diffuse intrinsic pontine glioma. *Front Oncol.* 2018;8(239):239.
16. Green AL, Flannery P, Hankinson TC, et al. Preclinical and clinical investigation of intratumoral chemotherapy pharmacokinetics in DIPG using gemcitabine. *Neurooncol Adv.* 2020;2(2):vdaa021.
17. Bobo RH, Laske DW, Akbasak A, et al. Convection-enhanced delivery of macromolecules in the brain. *Proc Natl Acad Sci U S A.* 1994;91(6):2076–2080.
18. de Vries NA, Beijnen JH, Boogerd W, van Tellingen O. Blood–brain barrier and chemotherapeutic treatment of brain tumors. *Expert Rev Neurother.* 2006;6(1):1199–1209.
19. Brady ML, Raghavan R, Alexander A, et al. Pathways of infusate loss during convection-enhanced delivery into the putamen nucleus. *Stereotact Funct Neurosurg.* 2013;91(2):69–78.
20. Mehta AM, Sonabend AM, Bruce JN. Convection-enhanced delivery. *Neurotherapeutics* 2017;14:358–371.
21. Anderson RCE, Kennedy B, Yanes CL, et al. Convection-enhanced delivery of topotecan into diffuse intrinsic brainstem tumors in children: report of 2 cases. *J Neurosurg Pediatr.* 2013;11(3):289–295.
22. Hynynen K, McDannold N, Vykhodtseva N, Jolesz FA. Noninvasive MR imaging–guided focal opening of the blood-brain barrier in rabbits. *Radiology.* 2001;220(3):640–646.
23. McDannold N, Arvanitis CD, Vykhodtseva N, Livingstone MS. Temporary disruption of the blood–brain barrier by use of ultrasound and microbubbles: safety and efficacy evaluation in rhesus macaques blood–brain barrier disruption via focused ultrasound. *Cancer Res.* 2012;72(14):3652–3663.
24. Liu H-L, Hua M-Y, Chen P-Y, et al. Blood-brain barrier disruption with focused ultrasound enhances delivery of chemotherapeutic drugs for glioblastoma treatment. *Radiology.* 2010;255(2):415–425.

25. Song K-H, Fan AC, Hinkle JJ, et al Microbubble gas volume: A unifying dose parameter in blood-brain barrier opening by focused ultrasound. *Theranostics*. 2016;7(1):144–152.
26. Borden MA, Song K-H. Reverse engineering the ultrasound contrast agent. *Adv Colloid Interface Sci*. 2018;262:39–49.
27. Stride E, Segers T, Lajoinie G, et al. Microbubble agents: new directions. *Ultrasound Med Biol*. 2020;46(6):1326–1343.
28. Song K-H, Harvey BK, Borden MA. State-of-the-art of microbubble-assisted blood-brain barrier disruption. *Theranostics*. 2018;8(16):4393–4408.
29. Helfield BL, Chen X, Qin B, Watkins SC, Villanueva FS. Mechanistic insight into sonoporation with ultrasound-stimulated polymer microbubbles. *Ultrasound Med Biol*. 2017;43(11):2678–2689.
30. Martinez P, Bottenus N, Borden M. Cavitation characterization of size-isolated microbubbles in a vessel phantom using focused ultrasound. *Pharmaceutics*. 2022;14(1925):1925.
31. Lentacker I, De Cock I, Deckers R, De Smedt SC, Moonen CTW. Understanding ultrasound induced sonoporation: definitions and underlying mechanisms. *Adv Drug Deliv Rev*. 2014;72:49–64.
32. McDannold N, Zhang Y, Supko JG, et al. Acoustic feedback enables safe and reliable carboplatin delivery across the blood-brain barrier with a clinical focused ultrasound system and improves survival in a rat glioma model. *Theranostics*. 2019;9(21):6284–6299.
33. Chu P-C, Chai W-Y, Tsai C-H, et al. Focused ultrasound-induced blood-brain barrier opening: association with mechanical index and cavitation index analyzed by dynamic contrast-enhanced magnetic-resonance imaging. *Sci Rep*. 2016;6(1):1–13.
34. Konofagou E, Tung YS, Choi J, et al. Ultrasound-induced blood-brain barrier opening. *Curr Pharm Biotechnol*. 2012;13(7):1332–1345.
35. Slingerland M, Hess D, Clive S, et al. A phase I, open-label, multicenter study to evaluate the pharmacokinetics and safety of oral panobinostat in patients with advanced solid tumors and various degrees of hepatic function. *Cancer Chemother Pharmacol*. 2014;74:1089–1098.
36. Hennika T, Hu G, Olaciregui NG, et al. Pre-clinical study of panobinostat in xenograft and genetically engineered murine diffuse intrinsic pontine glioma models. *PLoS One*. 2017;12(1):e0169485.
37. Balakrishnan I, Danis E, Pierce A, et al. Senescence induced by BMI1 inhibition is a therapeutic vulnerability in H3K27M-Mutant DIPG. *Cell Rep*. 2020;33(108286):108286.
38. Dahl NA, Danis E, Balakrishnan I, et al. Super elongation complex as a targetable dependency in diffuse midline glioma. *Cell Rep*. 2020;31(107485):107485.
39. Green AL, Ramkissoon SH, McCauley D, et al. Preclinical antitumor efficacy of selective exportin 1 inhibitors in glioblastoma. *Neuro Oncol*. 2015;17(5):697–707.
40. Feshitan JA, Chen CC, Kwan JJ, Borden MA. Microbubble size isolation by differential centrifugation. *J Colloid Interface Sci*. 2009;329(2):316–324.
41. Fedorov A, Beichel R, Kalpathy-Cramer J, et al. 3D slicer as an image computing platform for the Quantitative Imaging Network. *Magn Reson Imaging*. 2012;30(9):1323–1341.
42. Ishida J, Alli S, Bondoc A, et al. MRI-guided focused ultrasound enhances drug delivery in experimental diffuse intrinsic pontine glioma. *J Control Release*. 2021;330:1034–1045.
43. Haumann R, Bianco JI, Waranecki PM, et al. Imaged-guided focused ultrasound in combination with various formulations of doxorubicin for the treatment of diffuse intrinsic pontine glioma. *Transl Med Commun*. 2022;7(1):1–12.
44. Ghuman J, Zunszain PA, Petitpas I, et al. Structural basis of the drug-binding specificity of human serum albumin. *J Mol Biol*. 2005;353(1):38–52.
45. Van Veggel M, Westerman E, Hamberg P. Clinical pharmacokinetics and pharmacodynamics of panobinostat. *Clin Pharmacokinet*. 2018;57(1):21–29.
46. Harutyunyan AS, Chen H, Lu T, et al. H3K27M in gliomas causes a one-step decrease in H3K27 methylation and reduced spreading within the constraints of H3K36 methylation. *Cell Rep*. 2020;33(108390):108390.
47. Henrotte V, Vander Elst L, Laurent S, Muller RN. Comprehensive investigation of the non-covalent binding of MRI contrast agents with human serum albumin. *J Biol Inorg Chem*. 2007;12:929–937.
48. Damodharan S, Lara-Velazquez M, Williamsen BC, Helgager J, Dey M. Diffuse intrinsic pontine glioma: molecular landscape, evolving treatment strategies and emerging clinical trials. *J Pers Med*. 2022;12(5):840.
49. Zhang DY, Dmello C, Chen L, et al. Ultrasound-mediated delivery of paclitaxel for glioma: a comparative study of distribution, toxicity, and efficacy of albumin-bound versus cremophor formulations. *Clin Cancer Res*. 2020;26(2):477–486.
50. Arvanitis CD, Ferraro GB, Jain RK. The blood–brain barrier and blood–tumour barrier in brain tumours and metastases. *Nat Rev Cancer*. 2020;20(1):26–41.
51. Pi Z, Huang Y, Shen Y, et al. Sonodynamic Therapy on intracranial glioblastoma xenografts using sinoporphyrin sodium delivered by ultrasound with microbubbles. *Ann Biomed Eng*. 2019;47:549–562.
52. Englander ZK, Wei H-J, Pouliopoulos AN, et al. Focused ultrasound mediated blood–brain barrier opening is safe and feasible in a murine pontine glioma model. *Sci Rep*. 2021;11(6521):6521.
53. Wei H-J, Upadhyayula PS, Pouliopoulos AN, et al. Focused ultrasound-mediated blood-brain barrier opening increases delivery and efficacy of etoposide for glioblastoma treatment. *Int J Radiat Oncol*. 2021;110(2):539–550.
54. Alli S, Figueiredo CA, Golbourn B, et al. Brainstem blood brain barrier disruption using focused ultrasound: a demonstration of feasibility and enhanced doxorubicin delivery. *J Control Release*. 2018;281:29–41.
55. Ye D, Sultan D, Zhang X, et al. Focused ultrasound-enabled delivery of radiolabeled nanoclusters to the pons. *J Control Release*. 2018;283(1):143–150.
56. Anne M, de Sammartino D, Barginear M, Budman D. Profile of panobinostat and its potential for treatment in solid tumors: an update. *Onco Targets Ther*. 2013;1613:1613.
57. O'Reilly MA, Hynynen K. Blood-brain barrier: real-time feedback-controlled focused ultrasound disruption by using an acoustic emissions-based controller. *Radiology*. 2012;263(906):96–106.
58. Bing C, Hong Y, Hernandez C, et al. Characterization of different bubble formulations for blood-brain barrier opening using a focused ultrasound system with acoustic feedback control. *Sci Rep*. 2018;8(7986):7986.
59. Navarro-Becerra JA, Song K-H, Martinez P, Borden MA. Microbubble size and dose effects on pharmacokinetics. *ACS Biomater Sci Eng*. 2022;8(4):1686–1695.
60. Bunevicius A, McDannold NJ, Golby AJ. Focused ultrasound strategies for brain tumor therapy. *Oper Neurosurg*. 2020;19(1):9–18.
61. Papachristodoulou A, Signorell RD, Werner B, et al. Chemotherapy sensitization of glioblastoma by focused ultrasound-mediated delivery of therapeutic liposomes. *J Control Release*. 2019;295:130–139.
62. Franson A, Kline C, Molinaro A, et al. DIPG-09. Diffuse Midline Glioma-Adaptive Combinatory Trial (DMG-ACT): a biology-driven platform trial in pediatric and young adult patients with diffuse midline glioma. *Neuro Oncol*. 2022;24(Suppl 1):i19–i19.